Heliyon 10 (2024) e36777

Contents lists available at ScienceDirect

Heliyon

journal homepage: www.cell.com/heliyon

Research article

Multiaxial fatigue life assessment of dental implants

Mikel Armentia [a,b,*], Mikel Abasolo [a], Ibai Coria [a], Nicolas Saintier [c]

[a] Mechanical Engineering Department, University of the Basque Country (UPV/EHU), Bilbao, Spain
[b] R&D Department, Biotechnology Institute I mas D S.L., Miñano, Spain
[c] Institut de Mécanique et Ingénierie, École Nationale Supérieure d'Arts et Métiers, Bordeaux, France

ARTICLE INFO

Keywords:
Dental implants
Finite element analysis
Theory of critical distances
Critical plane methods
Design methodology

ABSTRACT

As screwed joints, dental restorations may suffer mechanical failures such as screw loosening and implant or prosthetic screw failure due to fatigue. This work is focused on the failure of the implant and develops a numerical methodology to predict its fatigue life under cyclic loading conditions. This methodology is based on the combination of Critical Plane Methods and the Theory of Critical Distances to account for stress multiaxiality and notch effects. The obtained predictions were validated experimentally, which can be used to identify the main geometrical, assembly and operational factors affecting the fatigue behavior of dental implants. As a result, a powerful and efficient design tool for fatigue life prediction of dental implants is presented. This methodology complements a previously presented one focused on the fatigue life prediction of the prosthetic screw, thereby, offering now a complete design tool package regardless the critical component of the dental restoration, predicting accurately the fatigue response of the restoration, with no need for long-term fatigue test campaigns. This is a pioneering work since no other fatigue design methodology for dental implants with such a solid foundation and experimental validation has been published to date.

1. Introduction

Oral rehabilitation based on implant-supported restorations represents a widespread practice to replace either a single missing dental piece or even a full arch of an edentulous patient [1]. The most commonly used restoration is composed by a dental implant, which is placed into the maxillar or mandibular bone, and an abutment. The abutment along with a previously cemented crown is then placed on the implant. Finally, a prosthetic screw is inserted and properly tightened in order to achieve structural integrity of the whole assembly (see Fig. 1).

Although the use of implant-based dental restorations is a highly reliable treatment, any case is susceptible to biological or mechanical complications. Together with screw self-loosening [2–6] and microgap formation [7–23], fatigue failure of implant or any of its prosthetic components is one of the most common mechanical problems [24–26]. Previous work presented a methodology for fatigue life prediction of regular or wide implants, where the prosthetic screw is usually the critical component [27], later validated experimentally on 4 implant supported restorations [28].

However, the industry of dental implantology is increasingly looking for narrower dental implants to deal with cases where the patient has little bone section. In case a narrow dental implant is used, the implant is likely to be critical component in terms of fatigue failure rather than the prosthetic screw, whose fatigue failure was previously studied by the authors in Refs. [27,28]. The fatigue

* Corresponding author. Mechanical Engineering Department, University of the Basque Country (UPV/EHU), Bilbao, Spain.
E-mail address: marmentia002@ikasle.ehu.eus (M. Armentia).

https://doi.org/10.1016/j.heliyon.2024.e36777
Received 31 January 2024; Received in revised form 8 August 2024; Accepted 22 August 2024
Available online 29 August 2024

analysis of the screw is relatively simple due to its geometry and uniaxial working condition that allow for the use of the uniaxial nominal stress value obtained straightforward from the formulation of the Theory of Elasticity. By contrast, implant body fatigue analysis may be considered more challenging because of its complex geometry and loads. In this case, multiaxial stresses with strong gradients show up at notch root of the outer implant thread where crack initiation occurs.

There are many publications regarding fatigue performance of dental restorations, most of them consisting of purely experimental works [29–34] often according to ISO 14801 standard [35]. In these studies the F-N curves (cyclic force vs fatigue life), or more commonly the fatigue life under a unique load level are provided, in order to find out which restoration behaves better under certain conditions. Some works also use Finite Element Analysis (FEA) [36–41], obtaining stress maps and correlating a higher peak stress under maximum load with a lower fatigue life without a rigorous fatigue live prediction methodology. This type of approach is understandable considering that these works are published in journals of the field of oral implantology whose target readers are clinicians. They usually are more interested in clinical implications of the different restorations designs available in the market than on an in-depth study of the fatigue phenomenon itself.

Although no works have been found that employ the theory of multiaxial fatigue for the study of dental implants, there is plenty of literature that presents the basis of multiaxial fatigue [42–44]. Papuga et al. besides compiling many of the multiaxial fatigue methods known so far, evaluate their accuracy [45]. Deng et al. on the other hand focuses on multiaxial fatigue under variable amplitude loads [46]. In the review, he compiles the basic concepts as well as classifies the latest achievements. Susmel focused on Theory of Critical Distances (TDC) and tested its accuracy under different loading conditions [47]. Shen et al. found in their paper that stress gradient and critical distance value are strongly related [48]. It should be noted that a dental restoration assembly is, in essence, a screwed joint. Its fatigue response should therefore be explainable and predictable by using the concepts and analysis methods developed in fatigue related scientific literature. Thus, the aim of this work is to apply these methodologies to the field of dental implantology, considering the particularities of narrow dental restorations, where the implant itself is commonly the critical component.

As a result, this paper develops and experimentally validates a methodology to predict fatigue life of dental implants. In this way, a consistent methodology for engineering departments is provided in terms of design optimization and experimental tests reduction. The methodology is based on standardized specimen tests to determine the fatigue behavior of the implant material and notch effect. Then, it analyzes the multiaxial stress condition at the specimen notch root combining Critical Plane Methods (CPM) and the TCD to predict the fatigue life of dental restorations under any conditions.

2. Methodology

The fatigue assessment methodology presented in this work combines CPM and TCD and its procedure is outlined in the following steps. In a first step, pure alternating axial fatigue tests were carried out on notched and unnotched standardized hourglass specimens. By means of these tests, material fatigue behavior is characterized and stress concentration effect (notch effect) is evaluated. In a second step, the local stress fields corresponding to the applied fatigue loading were obtained by FEA. Then the CPM combined with the Volume Method (VM) of TCD was used to calibrate critical distance value as a function of the normalized stress gradient. Based on those results, in a third step, a methodology which predicts the fatigue behavior of narrow dental restorations (where the implant is the fuse of the restoration). The following sections explain, respectively, these three steps.

2.1. Axial fatigue tests on standardized specimens

Pure alternating (R_{-1}) axial fatigue tests of standardized hourglass specimens [49–51] of CP4 titanium were performed, which is the material of the dental implants under study (chemical composition given in Table 1). Fatigue specimens were produced using the same bars used to create dental implants, so that the material used to manufacture the specimens is strictly identical to that used in the dental implants.

Fig. 2 (A - D) shows the drawings of the unnotched specimen as well as the three notched specimens. The unnotched specimen has a

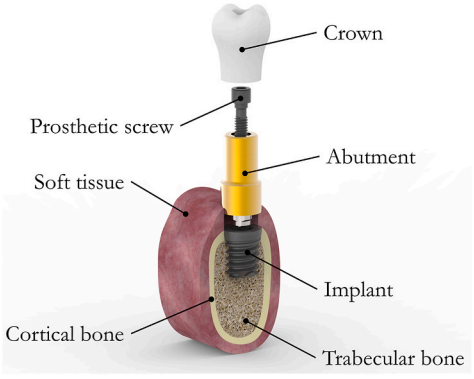

Fig. 1. A visual of an implant-supported restoration placed in a jawbone section.

Table 1
Ti6Al4V and CP4 Titanium composition.

Ti 6Al 4V ELI (GR5 Titanium)		CP4 Titanium	
Composition	**Wt. %**	**Composition**	**Wt. %**
Al	5.5–6.5	N(max)	0.05
V	3.5–4.5	C(max)	0.08
Fe(max)	0.25	Fe(max)	0.5
O(max)	0.13	O(max)	0.4
C(max)	0.08	H(max)	0.0125
N(max)	0.05	–	–
H(max)	0.012	–	–

3.5 mm neck diameter (critical section) while notched specimens have a 3 mm section diameter at the notch root and notch radii of 0.137 mm, 0.164 mm, and 0.650 mm. The notch radii were chosen so that the stress gradient located at the notch root for the three geometries bounds the ones computed in the critical zones of the dental implants. The stress concentration factor of each notch radius, based on the net section, is 3.1, 2.8, and 1.8 for notch radii of 0.137 mm, 0.164 mm, and 0.650 mm, respectively.

Fig. 3 shows the S-N curves composed by the fatigue data points obtained experimentally along with the regression models according to ASTM E739-91 [52]. This charts relate the nominal stress (i.e., not accounting for the stress concentration/gradient) in the critical section (force divided by net section) with the experimental fatigue life. The tests were carried out on a INSTRON 8801 servo-hydraulic test bench located at the Department of Mechanical Engineering (University of the Basque Country UPV-EHU, Bilbao, Spain). The linear regression models in Fig. 3 are virtually parallel, which involves that, for the material and notch geometries under study, the notch effect is independent of fatigue life (number of cycles). Thus from Fig. 3, the fatigue strength ratios, i.e. the relationship between the nominal stress ratios of notched specimens and the one of the unnotched specimen, turn out to be 2.1 for the R0.137 mm notch, 2.0 for the R0.164 mm notch and 1.43 for the R0.650 mm notch.

2.2. FEA of standardized specimens: critical distances and normalized stress gradients

The notch effect is accounted by using the TCD, reproducing the experimental load cases in Finite Element (FE) models. This approach consists of obtaining an effective stress σ_{eff} (also known as Fatigue Indicator Parameter (FIP) as defined in Ref. [53]) at a given distance (related to a critical distance d_c) from the root of the notch. This value is then used as the pertinent mechanical quantity to compute the fatigue life [47,54] of the notched sample from the unnotched S-N curve of the material as given in Fig. 3. Fig. 4 shows how stress is distributed along the notched section of a specimen and how the effective stress σ_{eff}, always higher than the nominal stress due to the influence of the notch effect, is located at a critical distance d_c. This critical distance can be identified using several methods such as the Point Method (PM), the Line Method (LM), the Area Method (AM) and the Volume Method (VM) (see Fig. 5(A–D)). PM defines σ_{eff} as the stress value at a point located at a distance d_{PM} from notch root. Alternatively, LM calculates σ_{eff} as the average stress on a straight line starting from the notch root to a distance d_{LM}. AM averages the stress within a well-defined area, in this case of a half circle with radius d_{AM} and centered at the notch root. Finally, VM calculates the average stress of a given volume, in this case defined as a sphere centered at the root of the notch with radius d_{VM}. PM, LM or AM are adequate for cases in which the direction (in the case of PM and LM) and the plane (in the case of AM) of the fatigue crack propagation is already known or can be easily predicted. However, in

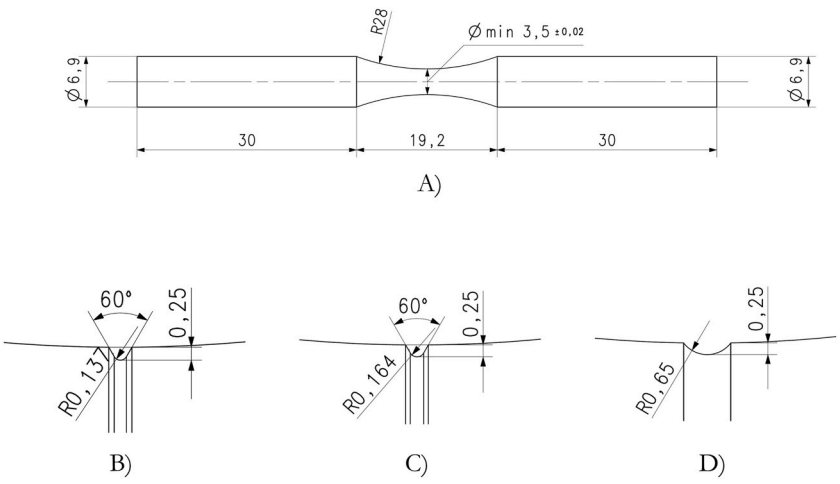

Fig. 2. Hourglass specimens used for material and notch effect characterization. A, Unnotched specimen. B, R0.137 notched specimen. C, R0.164 notched specimen. D, R0.650 notched specimen.

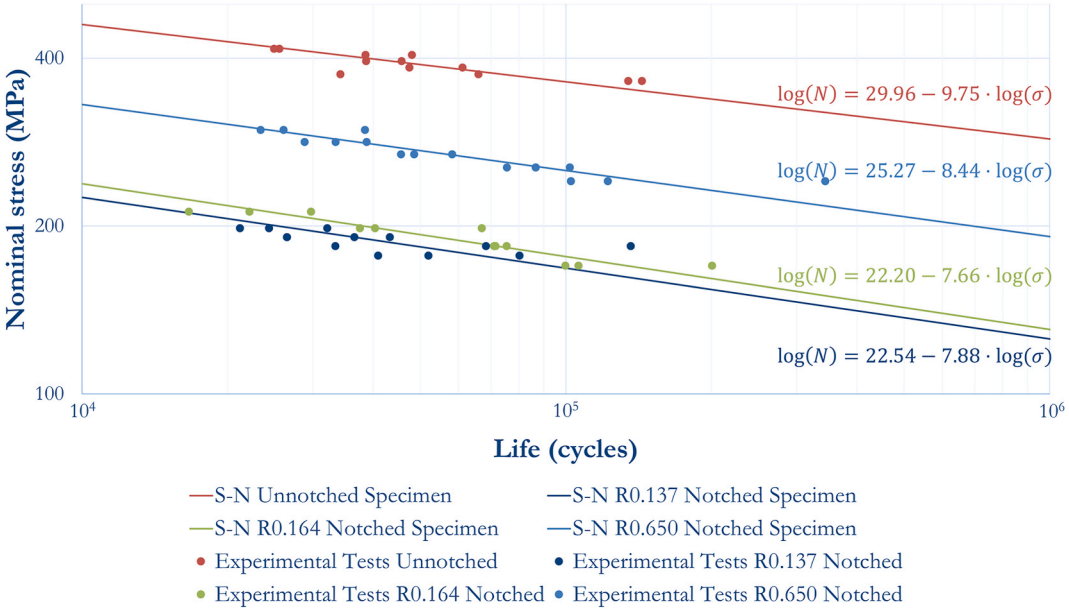

Fig. 3. Fatigue S-N curves of all tested specimens.

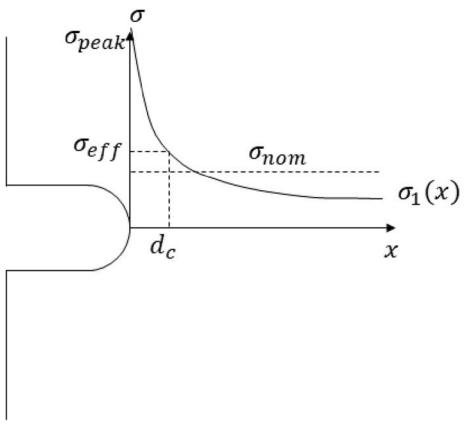

Fig. 4. TCD applied on a notched specimen to obtain an effective stress to account for fatigue calculations.

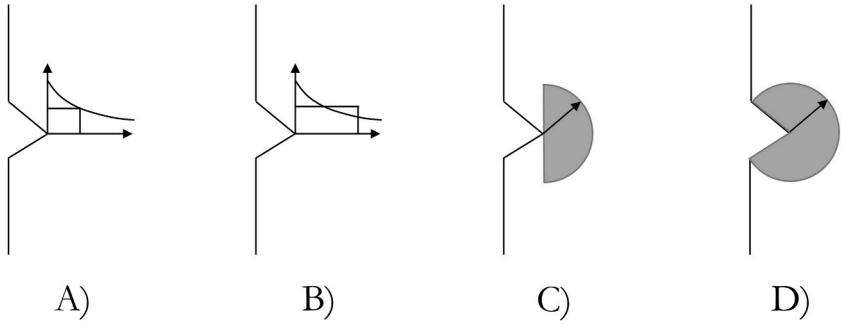

Fig. 5. Different methods based on the TCD. A, Point Method. B, Line Method. C, Area Method. D, Volume Method.

the case of a dental implant the crack propagation direction is hardly predictable due to the complexity of the geometry and loading conditions. Therefore, the VM was preferred as it does not presuppose a crack propagation direction and was found to give good results for complex multiaxial loadings or in the case of fatigue corrosion crack initiation from pits [53,55]. Thus, the FE models of the notched specimens were meshed in such a way that a sphere of 0.2 mm around the notch root was gradually refined as illustrated in Fig. 6 (A, B) for the R0.137 mm specimen. The material was modelled as linear elastic with a Young modulus E = 103,000 MPa and Poisson coefficient $\upsilon = 0.35$ [27].

A nominal stress of 1 MPa (force divided by net section of the critical section) was applied on the three FE models. From the FEA results, the stress field within the 0.2 mm-radius sphere was extracted, and the CPM of Findley and Dang Van were employed to obtain their associated equivalent stresses [44,45,47,56,57], calculated in Matlab R2019b. In brief, Findley method defines the critical plane as the one that satisfies equation (1) and uses the damage function of equation (2). With α and β being parameters obtained from alternating axial tests and alternating torsion tests (see equations (3) and (4)).

$$max_{n=1}^{p}(\tau_a + \alpha(\sigma_m + \sigma_a)) \tag{1}$$

$$\tau_{a_{eq}} = \tau_a + \alpha(\sigma_m + \sigma_a) < \beta \tag{2}$$

$$\alpha = \frac{2 - \frac{\sigma_{-1}}{\tau_{-1}}}{2\sqrt{\frac{\sigma_{-1}}{\tau_{-1}} - 1}} \tag{3}$$

$$\beta = \frac{\sigma_{-1}}{2\sqrt{\frac{\sigma_{-1}}{\tau_{-1}} - 1}} \tag{4}$$

Besides, Dang Van method identified the critical plane as the one meeting equation (5)and used the damage function in equation (6). With α and β being parameters obtained from equations (7) and (8).

$$max_{n=1}^{p}(\tau_a(t) + \alpha \cdot \sigma_h(t)) \tag{5}$$

$$\tau_{a_{eq}} = \tau_a(t) + \alpha \cdot \sigma_h(t) < \beta \tag{6}$$

$$\alpha = 3\left(\frac{\tau_{-1}}{\sigma_{-1}} - 0.5\right) \tag{7}$$

$$\beta = \tau_{-1} \tag{8}$$

Since all computations were performed using 1 MPa as a nominal stress, the obtained stress field and subsequent equivalent stress values are normalized values with respect to the nominal stress. Then, according to the VM, the effective stress σ_{eff}; that is, the averaged value of the stress, was determined as a function of the sphere radius (ranging from 0 mm to 0.2 mm), also normalized with respect to the nominal stress (see Fig. 7(A–C)). From the obtained effective stress σ_{eff} distributions, critical distance was defined as the distance at which σ_{eff} equals the aforementioned fatigue strength ratio. These values are 2.1 MPa for the R0.137 mm notch, 2.0 MPa for the R0.164 mm notch and 1.43 MPa for the R0.650 mm. As a result, the critical distances listed in Table 2 according to Findley and Dang Van criteria were obtained. As the critical distances are different for the three different notch geometries, the normalized stress gradient at the notch root was chosen as a suitable parameter to evaluate this variability. Table 3 shows the stress gradients for the

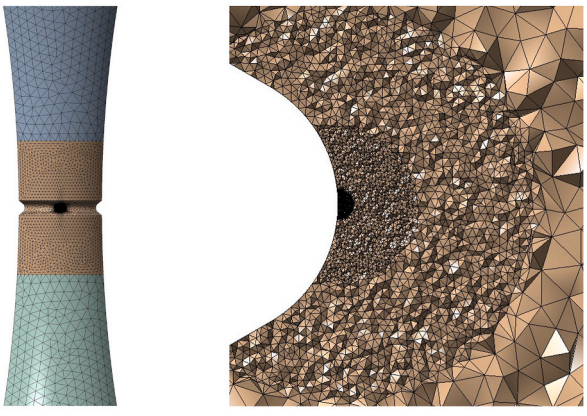

Fig. 6. FE model of the R0.650 mm notched hourglass specimen. A, Overview. B, Detail of the sphere-form progressive refinement at the root of the notch.

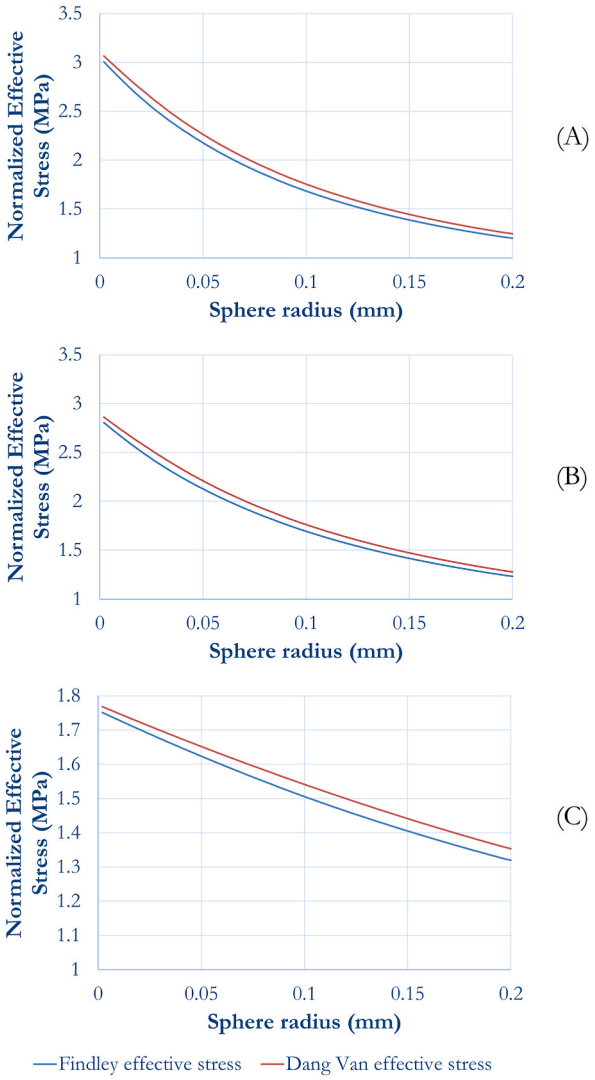

Fig. 7. Normalized effective stresses obtained though Findley and Dang Van methods ($\sigma_{eff}/\sigma_{nom}$) as function of the sphere radius (critical distance) for different notched specimens. A, R0.137 mm notch. B, R0.164 mm notch. C, R0.650 mm notch.

Table 2
Findley and Dang Van critical distances obtained for the three notch cases.

	Findley critical distance (mm)	Dang Van critical distance (mm)
R0.137 Notch	0.054	0.062
R0.164 Notch	0.061	0.069
R0.650 Notch	0.138	0.158

Table 3
Findley and Dang Van Normalized stress gradients for the three notch cases.

	Findley normalized stress gradient (mm^{-1})	Dang Van normalized stress gradient (mm^{-1})
R0.137 Notch	7.360	6.517
R0.164 Notch	6.191	5.494
R0.650 Notch	1.580	1.406

three different notch geometries divided by the maximum stress to obtain the normalized values. Then, a linear relationship between the critical distance d and the normalized stress gradient $\nabla\sigma$, plotted in Fig. 8, was proposed. Note that, since the proposed linear relationships are obtained from the combination of both theoretical and experimental approaches, the values of critical distances d obtained in Table 2 may vary due to the scatter inherent to experimental fatigue tests. Hence, as occurs with S-N curves, the trends in Fig. 8 may suffer variations if more experimental tests are performed. Furthermore, it should be mentioned that since only three different notch geometries were used in this study, linear seems to be the most rigorous regression, even though the test of more notch geometries may suggest more appropriate regression models.

2.3. Methodology for dental implants fatigue life prediction

Once the fatigue response and the notch effect of CP4 Titanium has been characterized with standardized hourglass specimens, the fatigue life of those dental implants made of that material can be predicted by following the methodology outlined in the flowchart of Fig. 9. Step 0 corresponds to the procedure described in previous sections. In step 1, a FEA of the dental restoration under study at a certain fatigue load is carried out. The details of such a model will be outlined in the next section. As has been done for the hourglass specimens, the stress results of the FE within a 0.2 mm-radius sphere centered at the crack initiation point, i.e., the notch root, are then obtained. These results must be computed for both the peak and valley values of the force since, as it may be expected, dental restorations do not work under pure alternating load as the specimens do. From the computed stress fields, the corresponding uniaxial equivalent stresses are obtained according to Findley or Dang Van criteria are obtained (step 2). Then, the effective stress σ_{eff} is computed for both criteria as a function of the sphere radius (ranging from 0 mm to 0.2 mm) as it was done for the hourglass specimens, obtaining a chart homologous to the one shown in Fig. 7(A–C), but, in this case, corresponding to the dental implant and fatigue load under study. Next, in step 3, the normalized stress gradient at the notch root is obtained, and the critical distance is determined according to the linear model proposed in Fig. 8. Finally, the effective stress σ_{eff} corresponding to that distance is calculated in step 4 so that, in step 5, the dental implant fatigue life is obtained from the S-N curve of the unnotched hourglass specimen.

This methodology is able to predict the fatigue behavior (number of cycles until failure) of any dental restoration regardless its geometry and working conditions (masticatory load, preload of the screw, etc) as long as the implant material is the same as the one characterized in step 0.

3. Experimental validation of the methodology on dental implants

The fatigue life of three different dental restorations under certain loading conditions were experimentally obtained. Then, the results were compared with the theoretical predictions from the methodology, in order to validate the presented fatigue life assessment methodology and verify its accuracy.

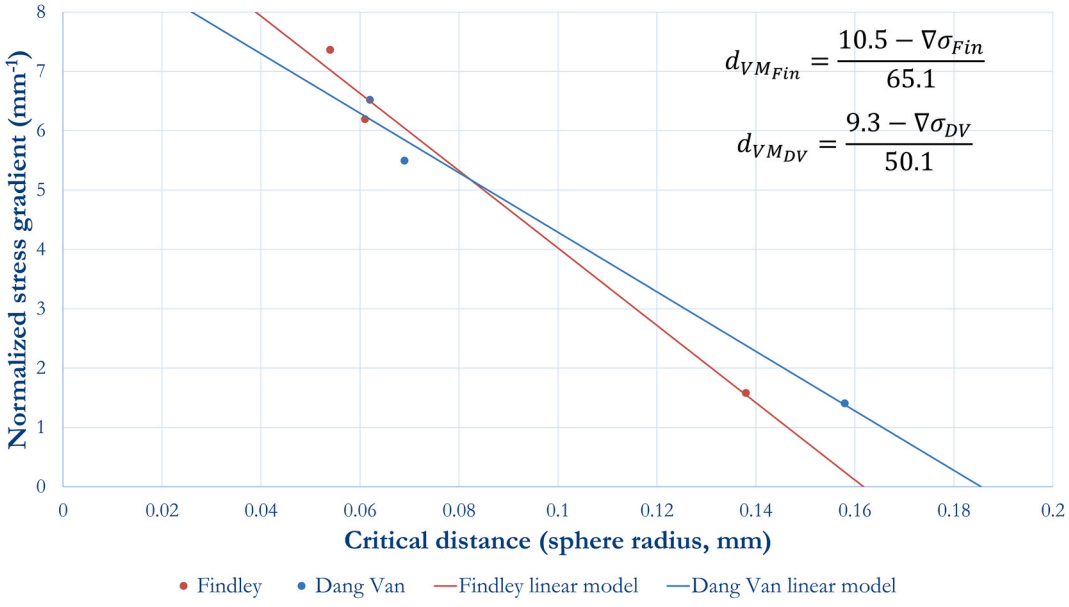

Fig. 8. Critical distance (sphere radius) as function of the normalized stress gradient for the three notch cases and the corresponding linear models proposed for Findley and Dang Van methods.

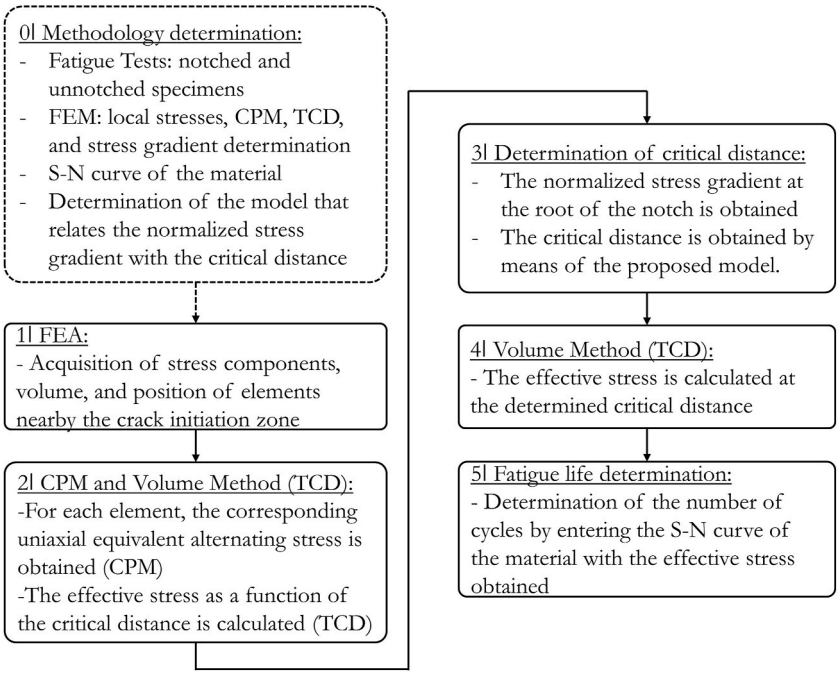

Fig. 9. Flowchart of the methodology proposed that predicts fatigue life of dental implants.

3.1. Experimental tests on dental restorations

Three different dental restorations were tested experimentally by performing fatigue loading until failure. All of them were composed of narrow implants so the implant itself was expected to be the critical component. The first restoration, from now on I-1, is composed by an IIPUCA3313 implant (BTI, Spain) with a butt-joint internal connection, Ø3.3 mm implant body and Ø4.1 mm platform, an INPPTU44 abutment and an INTTUH prosthetic screw with a M1.8 screw metric. The second dental restoration, from now on I-2, is composed by an IIP3CA3013 implant (BTI, Spain) with a butt-joint internal connection, Ø3mm implant body and Ø3mm platform, a INPPT3B34 abutment, and the aforementioned INTTUH prosthetic screw. The last dental restoration, from now on I-3, is composed by an IRTCA2513 (BTI, Spain) implant with an external connection, Ø2.5 mm implant body and Ø3.5 mm platform diameter. The abutment used in this third dental restoration is a PPATEB44 with a TTTH prosthetic screw with M2 screw metric. All of them were previously tested to verify that the dental implant was in fact the critical component, and to identify the crack initiation point. Fig. 10 (A - C) shows these restorations and Table 4 summarize their main features. The implants as well as the abutments are made of CP4 Titanium, the material tested in the standardized specimens, while the prosthetic screws are made of grade 5 Titanium (Ti6Al4V) (see Table 1).

The experimental fatigue tests were performed in an INSTRON E3000 Electropuls following the recommendations of the ISO 14801

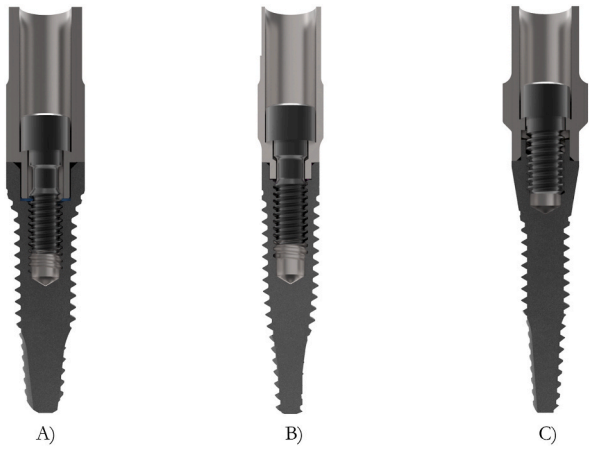

Fig. 10. The three implant-supported restoration models studied. A, I-1. B, I-2. C, I-3.

Table 4
Narrow implant-supported restorations under study.

Restoration	I-1	I-2	I-3
Implant	IIPUCA3313	IIP3CA3013	IRTCA2513
Abutment	INPPTU44	INPPT3B34	PPATEB44
Screw	INTTUH	INTTUH	TTTH
Body Ø (mm)	3.3	3.0	2.5
Platform Ø (mm)	4.1	3.0	3.5
IAC	Internal	Internal	External
Screw Metric	M1.8	M1.8	M2
Torque (Ncm)	35	35	35

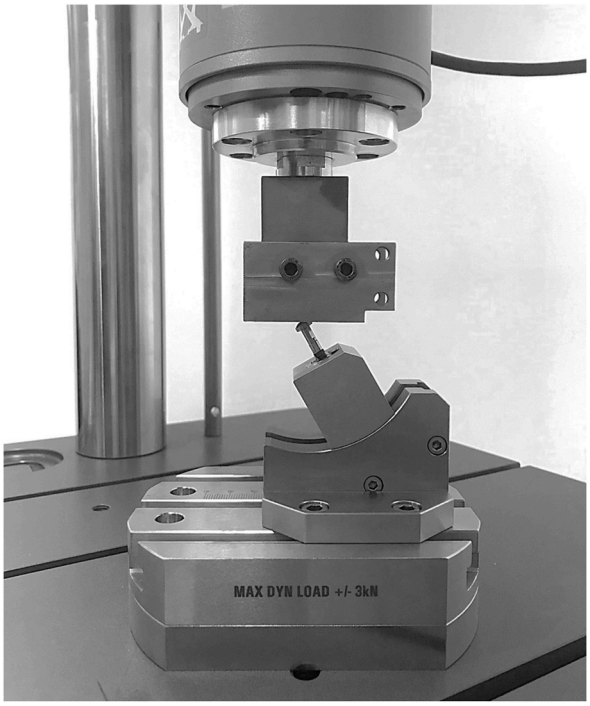

Fig. 11. INSTRON E3000 Electropuls fatigue test bench used for experimental testing according to ISO 14801 [35].

[35], a widely used Standard to characterize and certify the fatigue performance of dental restorations. Each abutment was mounted on its corresponding dental implant, then, the prosthetic screw was placed and tightened at 35Ncm. The dental restoration was inserted in a specimen holder, then glued and placed at 30° with respect to the load direction (vertical axis) as shown in Fig. 11. Then, cyclic load was applied until restoration failure. The load levels selected for each restoration were: $F_{max} = 220$N for I-1, 140N for I-2, and 130N for I-3, with a loading ratio R of 0.1. At those load values, 6 samples of I-1, 7 samples of I-2, and 7 samples of I-3 were tested. Fig. 12 (A - C) shows fatigue data points obtained experimentally. In all cases the implant failed at the thread positioned right below upper boundary of the specimen holder embedment, as illustrated in Fig. 13. Anderson-Darling test was carried out at each of the three cases studied, verifying that sample data does not significantly depart from a log-normal distribution (significance level of 0.05), therefore, log-normal distribution assumption cannot be rejected ($p = 0.5938$ for I-1, $p = 0.2243$ for I-2, and $p = 0.3219$ for I-3). Mean and Standard Deviation (SD) of logarithmic fatigue values for each dental restoration tests were: 4.63 and 0.18 for I-1, 4.42 and 0.29 for I-2, and 4.54 and 1.65 for I-3.

3.2. Methodology prediction of dental restorations

To compare these experimental fatigue life results with the theoretical predictions, FEA of the dental restorations were performed under same loading conditions. The complete geometry was modelled in order to allow for the application of the aforementioned fatigue design methodology. The threads of the prosthetic screw were modelled as cylindrical instead of helical, involving a negligible error in the stress results of the dental implant [27]. The external threads of the implant, though, were modelled as they are in reality; i.e., as helical. The abutment has undergone only one modification, the cut across its transverse section at 8 mm height from the implant platform. This modification was performed so that the load may directly be applied at the level specified in the ISO 14801 [35]

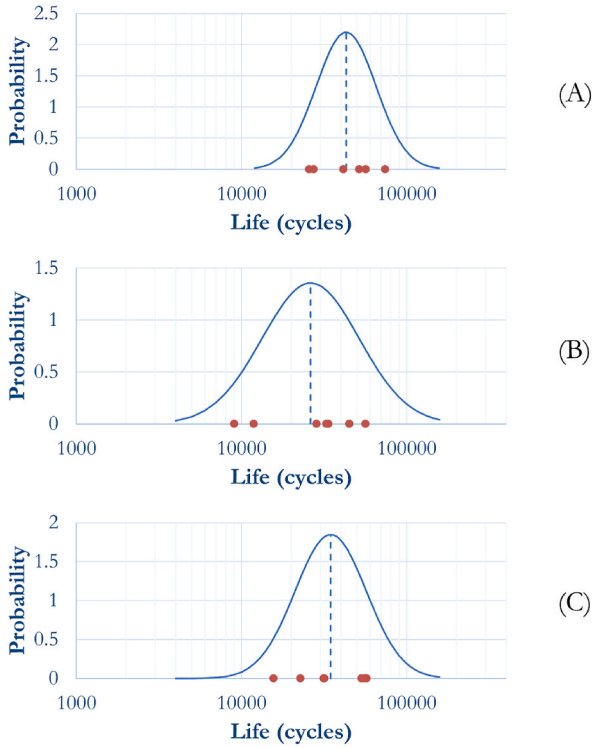

Fig. 12. Fatigue life obtained experimentally, its corresponding normal distribution function, and the average value. A, I-1 (220N). B, I-2 (140N). C, I-3 (130N).

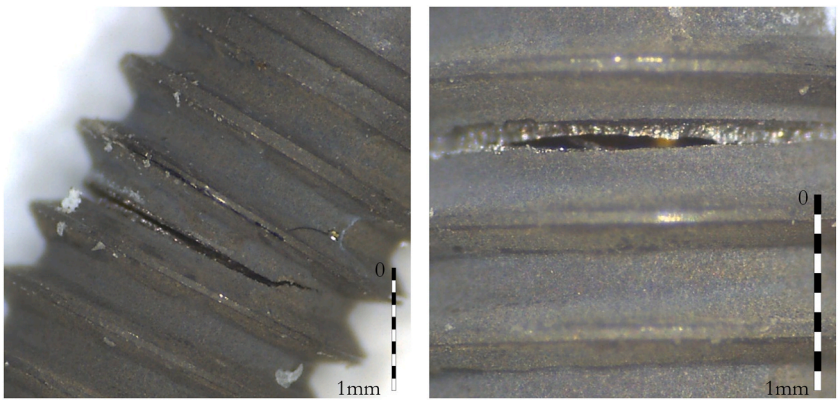

Fig. 13. Crack initiations located at the notch of the thread immediately below the implant embedment in the specimen (I-2).

mentioned above, avoiding the hemispherical device used in the experimental tests. Both materials, CP4 Titanium and Ti6Al4V, were modelled as linear elastic, with Young modulus being 103 GPa for both, and Poisson coefficient being $\nu = 0.35$ and $\nu = 0.31$, respectively [27]. Friction coefficient value of 0.17 was set for those contacts among the screw surfaces and the inner surfaces of both the implant and the abutment. Moreover, a friction coefficient value of 0.21 was set for those contacts among the surfaces that form the IAC [27]. In the experimental setup, the implant is placed in the specimen holder hole by previously being filled with an embedding material (Loctite 401), as recommended by ISO 14801 [35]. This particular boundary condition is modelled by setting a contact with a friction coefficient of 0.5. This condition allows for material deformation when either the preload is being applied or the implant is being compressed by the applied external load, while restricting lateral displacement.

The abutment and the screw-pretension section were meshed with second order hexahedra while second order tetrahedra were used in the rest of the bodies. 1 mm size elements were used for specimen holder meshing with a refinement on the implant contact surface by using 0.15 mm size elements. Both the abutment and the screw were meshed by using 0.1 mm size elements, with the last one having a refinement on the thread contact faces by using 0.025 mm elements. Implant meshing was performed by using 0.1 mm

elements and refining the mesh by using 0.025 mm elements on inner thread surfaces. Finally, the implant had a sphere-form progressive refinement with the center being located at the notch root where the crack starts. The first refinement sphere used 0.03 mm size elements with a radius of 0.3 mm. Then, the second refinement sphere used 0.008 mm size elements with a radius of 0.2, followed by a third sphere that used 0.004 mm size elements with a radius of 0.08 mm. Finally, the last refinement sphere used 0.001 mm size elements with a radius of 0.02. Fig. 14 (A, B) shows both the FE model and the detail of the sphere refinement at the root of the notch, i.e. the crack initiation point, for one of the dental restorations under study. Regarding the boundary conditions, fixed supports were applied at the base and side of the specimen holder as well as at the base of the implant. The FEA consisted of two load steps. In the first step, the preload corresponding to 35Ncm tightening torque was applied on the screw. The values of the preload for the three cases are: 814N for I-1 and for I-2, and 761N for I-3, obtained as explained in previous work [27].

Fig. 15 (A - C) shows the Von Mises stresses for each of the three implants under study under the maximum applied load (F_{max} = 220N, 140N and 130N for I-1, I-2, and I-3, respectively). As mentioned, the stress field within the sphere was obtained for the experimentally applied loadings and a loading ratio R of 0.1. Next, Findley and Dang Van equivalent alternating stresses of those elements were calculated. Then, the effective stress as a function of the sphere radius (see Fig. 16(A–C)) as well as the normalized stress gradient values at the notch root (see Table 5) were obtained for each dental restoration. The values of Table 5 were then used to enter the linear model presented Fig. 8 in order to calculate the critical distance to be used for each dental implant, with the results in Table 6. Note that the normalized stress gradients of the implants fell within the range of the normalized stress gradients of the specimens.

Using the critical distance values of Table 6 together with Fig. 16(A–C), the effective fatigue stresses listed in Table 7 were obtained. Finally, these stress values were used to predict the fatigue life by entering the S-N curve of the unnotched specimen in Fig. 3. Thus, Fig. 17 (A, B) shows these theoretical predictions according to Findley and Dang Van (CPM) as well as the material S-N (unnotched specimen) that obviously matches the 3 prediction points. The experimental fatigue life results are also showed, including the average value and its log-normal probability function. It can be observed that the theoretical predictions by the methodology developed in this work accurately fit the results obtained experimentally for all the dental restorations studied, with Findley method being more conservative than Dang Van method for the cases under study.

4. Discussion

This work developed a methodology to assess the fatigue life of narrow dental restorations; i.e., restorations in which the mechanical fuse is the dental implant. It combines state-of-art fatigue calculation methods such as CPM and TCD, taking as starting point uniaxial fatigue tests of different specimens to determine material fatigue behavior.

Regarding the notch effect, specimen tests showed that, for the material and notch geometries under study, the reduction of the fatigue resistance in the S-N curve is independent of the number of cycles. For other materials or notch geometries with stress gradients significantly different from the ones studied in this work, the notch effect may be sensitively different, so experimental tests should be carried out to feed the methodology correspondingly. Based upon this material characterization, the TCD was used to calculate an effective stress, using VM as the most reasonable alternative for cases like the one under study in which the crack propagation direction is difficult to foresee. However, other approaches such as the PM with less computational cost could be used analyzing different potential propagation paths [47]. Besides, in principle the TCD was developed for infinite life calculation; that is, to establish if a component would or not suffer fatigue failure, and therefore the critical distance was set as a material property (as well as the load ratio R). Nevertheless, Susmel experimentally validated its use for finite life assuming a linear relationship in log-log scale between fatigue

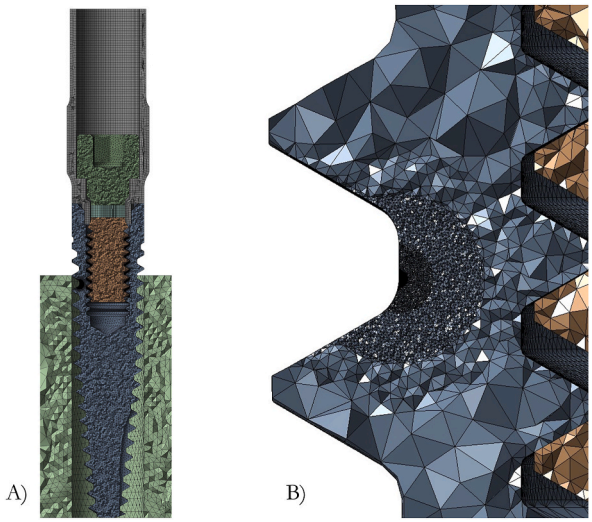

Fig. 14. A, Meshed model of I-2 dental implant and its prosthetic components. B, Detail of the sphere-form refinement at the notch root.

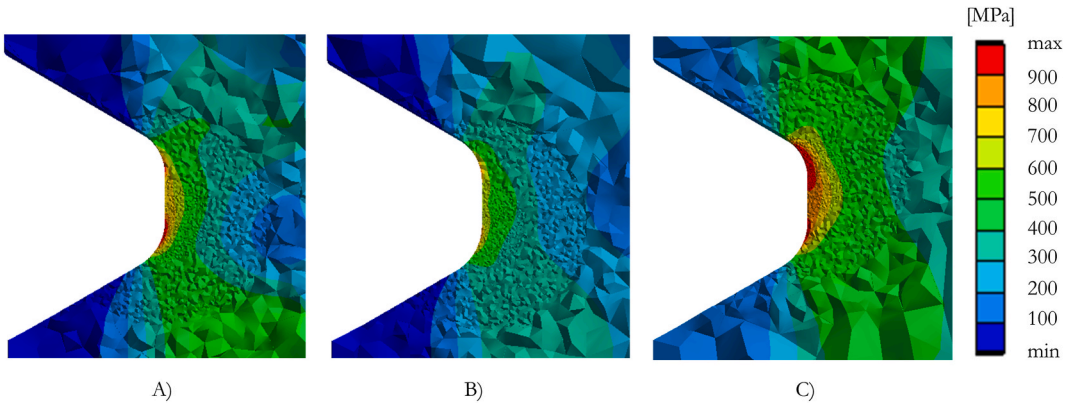

Fig. 15. Von Mises stresses at the root of the notch of each of the three implants analyzed. A, I-1 (220N). B, I-2 (140N). C, I-3 (130N). Element edges (usually in black) are not shown to allow the correct visualization of the stresses, especially at the root of the notch there the mesh is extremely refined.

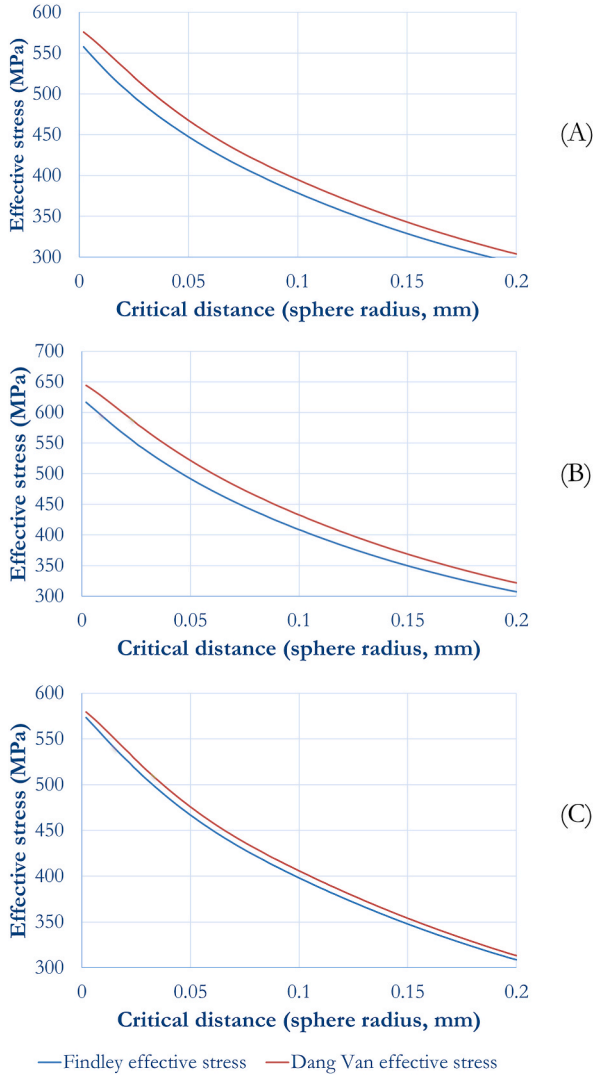

Fig. 16. Effective stresses for Findley and Dang Van methods as function of the critical distance (sphere radius) (critical distance). A, I-1. B, I-2. C, I-3.

Table 5
Normalized stress gradient values at the notch root for the three dental restorations studied.

	Findley normalized stress gradient (mm^{-1})	Dang Van normalized stress gradient (mm^{-1})
I-1	5.420	3.636
I-2	4.914	3.607
I-3	4.449	3.486

Table 6
Critical distance values for the three dental restorations studies.

	Findley critical distance (mm)	Dang Van critical distance (mm)
I-1	0.079	0.113
I-2	0.086	0.114
I-3	0.092	0.115

Table 7
Effective stress values for the three dental restorations studied.

	Findley effective stress (MPa)	Dang Van effective stress (MPa)
I-1	405.6	380.1
I-2	429.0	412.5
I-3	407.4	389.1

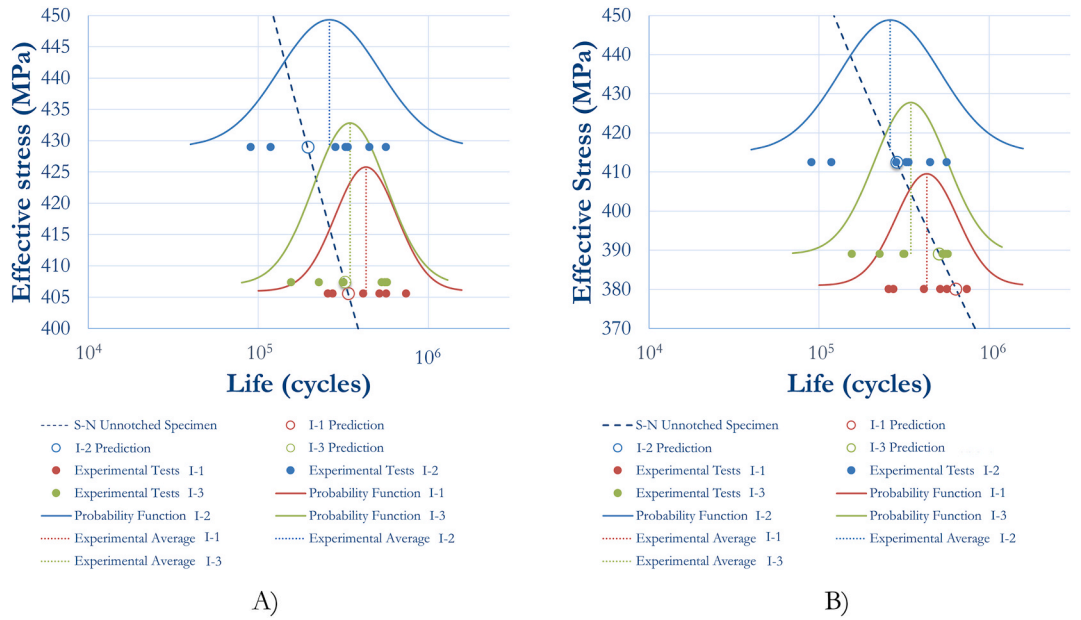

Fig. 17. Experimental fatigue life of each dental implant and their corresponding fatigue life prediction obtained from the proposed methodology. A, Findley. B, Dang Van.

life (number of cycles) and critical distance [47]. More recently, other works claimed that critical distance also depends on notch geometry. In this sense, they adapted the aforementioned "critical distance vs number of cycles" equation by Susmel [47] including the values of the theoretical stress concentration factor or the normalized stress gradient in order to account for the notch effect [48]. In the present work, for the material, geometry and working conditions under study, the critical distance was found to be independent of the number of cycles. This is explained by the fact that the critical distance is closely related to the fatigue strength ratio. Therefore, if the fatigue strength ratio is constant over the cycles, so will be the critical distance. Hence, the critical distance was dependent only on the notch geometry; to this extent, a linear relationship between critical distance and normalized stress gradient was proposed. Even though the results of the methodology are satisfactory, even higher accuracy could be expected if more notch geometries were tested to obtain a potentially more representative 'critical distance vs stress gradient' relationship.

Regarding multiaxial fatigue methods, even though CPM were initially developed for infinite life, they may also be used for finite

life calculations [42] if only very little cyclic plasticity occurs at the notch root during cyclic loading. In this work, Findley and Dang Van equivalent stresses were used, however other multiaxial fatigue methods could provide similar results [45].

5. Conclusions

A methodology for the fatigue life calculation of implant restorations in which the dental implant is the mechanical fuse was developed. Due to its complex geometry and loading condition, the stress status in dental implants is multiaxial and notch effects are of great importance. Thus, a simple nominal stress approach like the one presented in previous work by the authors for the fatigue life assessment of prosthetic screws is not valid in this case. Therefore, the methodology numerically calculates the multiaxial stress components via FEA, and obtains an alternating equivalent stress using state-of-art Critical Plane Methods. In order to consider the notch effect, the effective stress value was obtained by means of the Theory of the Critical Distance, with the Volume Method to account for any possible crack propagation direction. In this sense, standardized hourglass-shaped material specimens showed that, in this case, the critical distance value does not depend on fatigue life. However, it varies with the normalized stress gradient at the crack initiation point, following a linear relationship proposed by the authors for this case.

The fatigue life predicted by the methodology was further validated with experimental fatigue tests on three different dental restorations, with satisfactory results. Further research will aim to simplify the methodology, for example using Point Method instead of Volume Method, or von Mises stress instead of Critical Plane Methods. This will decrease the computational cost of the methodology, but presumably at the cost of a loss of precision.

Data availability statement

The authors do not have permission to share further data.

CRediT authorship contribution statement

Mikel Armentia: Writing – review & editing, Writing – original draft, Visualization, Validation, Methodology, Investigation. **Mikel Abasolo:** Methodology, Investigation, Conceptualization. **Ibai Coria:** Supervision, Software, Data curation. **Nicolas Saintier:** Validation, Supervision, Resources.

Declaration of competing interest

The authors declare the following financial interests/personal relationships which may be considered as potential competing interests: The research group reports financial support was provided by the University of the Basque Country through the project LTC AENIGME [COLAB19/04] and Basque Government, Spain [grant number IT1542-22]. Mikel Armentia reports a relationship with BTI ImasD S.L. that includes: employment. If there are other authors, they declare that they have no known competing financial interests or personal relationships that could have appeared to influence the work reported in this paper.

References

[1] A. Warreth, H. Fesharaki, R. McConville, D. McReynolds, An introduction to single implant abutments, Dent. Update 40 (2013) 7–17.
[2] R.A. Stüker, E.R. Teixeira, J.C.P. Beck, N.P. Da Costa, Preload and torque removal evaluation of three different abutment screws for single standing implant restorations, J. Appl. Oral Sci. 16 (2008) 55–58.
[3] H.A. Zeno, R.L. Buitrago, S.S. Sternberger, M.E. Patt, N. Tovar, P. Coelho, K.S. Kurtz, F.J. Tuminelli, The effect of tissue entrapment on screw loosening at the implant/abutment interface of external- and internal-connection implants: an in vitro study, J. Prosthodont. 25 (2016) 216–223.
[4] T. Paepoemsin, P.A. Reichart, P. Chaijareenont, F.P. Strietzel, P. Khongkhunthian, Removal torque evaluation of three different abutment screws for single implant restorations after mechanical cyclic loading, Oral Implantol (Rome) 9 (2016) 213–221.
[5] M.S. Schwarz, Mechanical complications of dental implants, Clin. Oral Implants Res. 11 (2000) 156–158.
[6] M.-D. Jeng, Y.-S. Lin, C.-L. Lin, Biomechanical evaluation of the effects of implant neck wall thickness and abutment screw size: a 3D nonlinear finite element analysis, Appl. Sci. 10 (2020) 3471.
[7] J. Lindhe, T. Berglundh, I. Ericsson, B. Liljenberg, C. Marinello, Experimental breakdown of peri-implant and periodontal tissues. A study in the beagle dog, Clin. Oral Implants Res. 3 (1992) 9–16.
[8] N. Broggini, L.M. McManus, J.S. Hermann, R.U. Medina, T.W. Oates, R.K. Schenk, D. Buser, J.T. Mellonig, D.L. Cochran, Persistent acute inflammation at the implant-abutment interface, J. Dent. Res. 82 (2003) 232–237.
[9] M. Rismanchian, M. Hatami, H. Badrian, N. Khalighinejad, H. Goroohi, Evaluation of microgap size and microbial leakage in the connection area of 4 abutments with straumann (ITI) implant, J. Oral Implantol. 38 (2012) 677–685.
[10] L. Steinebrunner, S. Wolfart, K. Bössmann, M. Kern, In vitro evaluation of bacterial leakage along the implant-abutment interface of different implant systems, Int. J. Oral Maxillofac. Implants 20 (2005) 875–881.
[11] P. Khongkhunthian, S. Khongkhunthian, W. Weerawatprachya, K. Pongpat, W. Aunmeungtong, Comparative study of torque resistance and microgaps between a combined Octatorx-cone connection and an internal hexagon implant-abutment connection, J. Prosthet. Dent 113 (2015) 420–424.
[12] M. Fernández, L. Delgado, M. Molmeneu, D. García, D. Rodríguez, Analysis of the misfit of dental implant-supported prostheses made with three manufacturing processes, J. Prosthet. Dent 111 (2014) 116–123.
[13] J. Aguirrebeitia, M. Abasolo, J. Vallejo, R. Ansola, Dental implants with conical implant-abutment interface: influence of the conical angle difference on the mechanical behavior of the implant, Int. J. Oral Maxillofac. Implants 28 (2013) e72–e82.
[14] N. Broggini, L.M. McManus, J.S. Hermann, R. Medina, R.K. Schenk, D. Buser, D.L. Cochran, Peri-implant inflammation defined by the implant-abutment interface, J. Dent. Res. 85 (2006) 473–478.
[15] A.D. Boynueğri, M. Yalim, S.K. Nemli, B.I. Ergüder, P. Gökalp, Effect of different localizations of microgap on clinical parameters and inflammatory cytokines in peri-implant crevicular fluid: a prospective comparative study, Clin Oral Investig 16 (2012) 353–361.

[16] F. Carinci, A. Girardi, A. Palmieri, M. Martinelli, L. Scapoli, A. Avntaggiato, G.M. Nardi, D. Lauritano, Peri-Implantitis and bacteriological analysis, Eur. J. Inflamm. 10 (2012) 91–93.
[17] J.S. Hermann, D. Buser, R.K. Schenk, D.L. Cochran, Crestal bone changes around titanium implants. A histometric evaluation of unloaded non-submerged and submerged implants in the canine mandible, J. Periodontol. 71 (2000) 1412–1424.
[18] J.S. Hermann, D.L. Cochran, P.v. Nummikoski, D. Buser, Crestal bone changes around titanium implants. A radiographic evaluation of unloaded nonsubmerged and submerged implants in the canine mandible, J. Periodontol. 68 (1997) 1117–1130.
[19] M. Gross, I. Abramovich, E. Weiss, Microleakage at the abutment-implant interface of osseointegrated implants: a comparative study, Int. J. Oral Maxillofac. Implants 14 (1999) 94–100.
[20] P. Galindo-Moreno, A. León-Cano, I. Ortega-Oller, A. Monje, F. O'valle, A. Catena, Marginal bone loss as success criterion in implant dentistry: beyond 2 mm, Clin. Oral Implants Res. 26 (2015) e28–e34.
[21] F. Carinci, D. Lauritano, F. Cura, M.A. Lopez, M.A. Bassi, L. Confalone, F. Pezzetti, Prevention of bacterial leakage at implant-Abutment connection level: an in vitro study of the efficacy of three different implant systems, J. Biol. Regul. Homeost. Agents 30 (2016) 69–73.
[22] T.-J. Oh, J. Yoon, C.E. Misch, H.-L. Wang, The causes of early implant bone loss: myth or science? J. Periodontol. 73 (2002) 322–333.
[23] D. Weng, M.J.H. Nagata, M. Bell, A.F. Bosco, L.G.N. de Melo, E.J. Richter, Influence of microgap location and configuration on the periimplant bone morphology in submerged implants. An experimental study in dogs, Clin. Oral Implants Res. 19 (2008) 1141–1147.
[24] J.M. Ayllón, C. Navarro, J. Vázquez, J. Domínguez, Fatigue life estimation in dental implants, Eng. Fract. Mech 123 (2014) 34–43.
[25] M. Abasolo, J. Aguirrebeitia, J. Vallejo, J. Albizuri, I. Coria, Influence of vertical misfit in screw fatigue behavior in dental implants: a three-dimensional finite element approach, Proc. Inst. Mech. Eng. H 232 (2018) 1117–1128.
[26] K. Shemtov-Yona, D. Rittel, Fatigue of dental implants: facts and fallacies, Dent. J. 4 (2016) 1–16.
[27] M. Armentia, M. Abasolo, I. Coria, J. Albizuri, Fatigue design of dental implant assemblies: a nominal stress approach, Metals 10 (2020) 744.
[28] M. Armentia, M. Abasolo, I. Coria, N. Sainitier, Effect of the geometry of butt-joint implant-supported restorations on the fatigue life of prosthetic screws, J. Prosthet. Dent 127 (2022) 477.e1–477.e9.
[29] K. Shemtov-Yona, D. Rittel, E.E. Machtei, L. Levin, E.E. Machtei, L. Levin, E.E. Machtei, Effect of dental implant diameter on fatigue performance. Part I: mechanical behavior, Clin. Implant Dent. Relat. Res. 16 (2014) 172–177.
[30] H. Fan, X. Gan, Z. Zhu, Evaluation of dental implant fatigue performance under loading conditions in two kinds of physiological environment, Int. J. Clin. Exp. Med. 10 (2017) 6369–6377.
[31] A.I. Nicolas-Silvente, E. Velasco-Ortega, I. Ortiz-Garcia, A. Jimenez-Guerra, L. Monsalve-Guil, R. Ayuso-Montero, J. Gil, J. Lopez-Lopez, Influence of connection type and platform diameter on titanium dental implants fatigue: non-axial loading cyclic test analysis, Int. J. Environ. Res. Publ. Health 17 (2020) 8988.
[32] S. Dittmer, M.P. Dittmer, P. Kohorst, M. Jendras, L. Borchers, M. Stiesch, Effect of implant-abutment connection design on load bearing capacity and failure mode of implants, J. Prosthodont. 20 (2011) 510–516.
[33] A. Khraisat, R. Stegaroiu, S. Nomura, O. Miyakawa, Fatigue resistance of two implant/abutment joint designs, J. Prosthet. Dent 88 (2002) 604–610.
[34] Fernández Asián, Martínez González, Torres Lagares, Serrera Figallo, Gutiérrez Pérez, External connection versus internal connection in dental implantology. A mechanical in vitro study, Metals 9 (2019) 1106.
[35] ISO 14801:2007, Dentistry, Implants. Dynamic Fatigue Test for Endosseous Dental Implants, International Organization for Standardization, Geneva, Switzerland, 2007.
[36] J.F. Santiago Junior, E.P. Pellizzer, F.R. Verri, P.S.P. De Carvalho, Stress analysis in bone tissue around single implants with different diameters and veneering materials: a 3-D finite element study, Mater. Sci. Eng. C 3 (2013) 4700–4714.
[37] S.H. Chang, C.L. Lin, S.S. Hsue, Y.S. Lin, S.R. Huang, Biomechanical analysis of the effects of implant diameter and bone quality in short implants placed in the atrophic posterior maxilla, Med. Eng. Phys. 34 (2012) 153–160.
[38] L. Himmlová, T. Dostálová, A. Kácovský, S. Konvičková, Influence of implant length and diameter on stress distribution: a finite element analysis, J. Prosthet. Dent 91 (2004) 20–25.
[39] B. Georgiopoulos, K. Kalioras, C. Provatidis, M. Manda, P. Koidis, The effects of implant length and diameter prior to and after osseointegration: a 2-D finite element analysis, J. Oral Implantol. 33 (2007) 243–256.
[40] L. Baggi, I. Cappelloni, M. Di Girolamo, F. Maceri, G. Vairo, The influence of implant diameter and length on stress distribution of osseointegrated implants related to crestal bone geometry: a three-dimensional finite element analysis, J. Prosthet. Dent 100 (2008) 422–431.
[41] L. Minatel, F.R. Verri, G.A.H. Kudo, D.A. de Faria Almeida, V.E. de Souza Batista, C.A.A. Lemos, E.P. Pellizzer, J.F. Santiago, Effect of different types of prosthetic platforms on stress-distribution in dental implant-supported prostheses, Mater. Sci. Eng. C 71 (2017) 35–42.
[42] D. Socie, Multiaxial Fatigue, SAE International, 1999. Warrendale, PA.
[43] R.I. Stephens, A. Fatemi, Metal Fatigue in Engineering, second ed., Wiley, 2000.
[44] R. Avilés Gonzalez, in: Métodos de cálculo de fatiga para ingeniería. Metales, first ed., 2015. Paraninfo.
[45] J. Papuga, A survey on evaluating the fatigue limit under multiaxial loading, Int. J. Fatig. 33 (2011) 153–165.
[46] Q.Y. Deng, S.P. Zhu, J.C. He, X.K. Li, A. Carpinteri, Multiaxial fatigue under variable amplitude loadings: review and solutions, International Journal of Structural Integrity 13 (2022).
[47] L. Susmel, The theory of critical distances: a review of its applications in fatigue, Eng. Fract. Mech. 75 (2008) 1706–1724.
[48] J. Shen, H. Fan, G. Zhang, R. Pan, J. Wang, Z. Huang, Influence of the stress gradient at the notch on the critical distance and life prediction in HCF and VHCF, Int. J. Fatig. 162 (2022) 107003.
[49] ASTM E-466, Standard Practice for Conducting Force Controlled Constant Amplitude Axial Fatigue Tests of Metallic Materials (2015).
[50] ISO 1099, Metallic materials — Fatigue testing — Axial force-controlled method (2017).
[51] DIN 50100, Execution and evaluation of cyclic tests at constant load amplitudes (2016).
[52] ASTM E-739, Standard practice for statistical analysis of linear or linearized stress-life (S–N) and strain-life (e–N) fatigue data (2004).
[53] B. Vayssette, N. Saintier, C. Brugger, M. El May, E. Pessard, Numerical modelling of surface roughness effect on the fatigue behavior of Ti-6Al-4V obtained by additive manufacturing, Int. J. Fatig. 123 (2019) 180–195.
[54] D. Taylor, The Theory of Critical Distances, Elsevier Ltd, 2007.
[55] N. Saintier, T. Palin-luc, J. Bénabes, F. Cocheteux, Non-local energy based fatigue life calculation method under multiaxial variable amplitude loadings, Int. J. Fatig. 54 (2013) 68–83.
[56] G.I. Taylor, Plastic Strain in Metals, Twenty-Eighth May Lecture to the Institute of Metals, 1938.
[57] T.H. Lin, Analysis of elastic and plastic strains of a face-centred cubic crystal, J Mech Phys Solids 5 (1957).